Ultrasonic Backscattering in Duplex Microstructures: Theory and Application to Titanium Alloys

Y.K. HAN and R.B. THOMPSON

A theory is presented for the ultrasonic backscattering in duplex microstructures. Assuming single scattering described by the Born approximation, we consider a microstructure consisting of macrograins containing colonies with crystallographically related orientations. General results are presented for the backscattering coefficient, assuming that all variants occur with equal probability. These are then applied to the particular case of titanium alloys, in which the macrograins are taken to be prior beta grains and the colonies are assumed to be alpha phase produced by a martensitic transformation. Numerical results illustrate the effects of ultrasonic frequency, colony size and ellipticity, and macrograin size and ellipticity on the backscattering.

I. INTRODUCTION

THE propagation of ultrasonic waves in polycrystals is of broad interest. The immediate motivation for the present work is found in nondestructive evaluation. When ultrasound is used to detect flaws, the individual crystallites will scatter a portion of the incident energy, leading to an attenuation of the beam and creating a backscattered signal[1] that can mask the signals reflected from small flaws.[2] The backscattered signals also have been used to advantage in material characterization studies, in which they have been analyzed to obtain information on such structural features as grain size and porosity.[1,3] However, despite the obvious technological importance of the backscattering, the relationship of this ultrasonic property to microstructure is not well understood. For example, in commercial titanium alloys such as Ti-6Al-4V, large anisotropies in the backscattering are often observed, with no corresponding anisotropic features being observed in optical or scanning electron microscopy (SEM) micrographs.[2] It has been speculated that the anisotropic noise is related to local variations in texture and/or the shapes of the features revealed by macroetches. However, no careful theory has been presented to quantitatively describe these relationships. In this article, a theory is presented and applied to an idealized microstructure. The results are believed to provide important insight into the relationship of backscattered noise and microstructure.

For the case of single-phase materials, considerable work already has been done with early efforts directed at attenuation. In this case, scattering is caused by acoustic impedance fluctuations, which are directly related to orientations of crystallites or grains. Lifshits and Parkhomovskii,[4,5] Bhatia,[6,7] and Bhatia and Moore[8] investigated attenuation, including results for arbitrarily shaped scatterers in the Rayleigh-scattering regime ($\lambda >> d$). At higher frequencies, Rokhlin[9] studied cubical scatterers in both the stochastic ($d \sim \lambda$) and the diffuse ($d >> \lambda$) scattering regions. Other important early results include the consideration of two-phase systems by Truell *et al.*[10] and multiple scattering by Watermann and Truell.[11] Papadakis provides a review of much of the early work.[12] Important recent contributions, including the work of Hirsekorn,[13–17] and Stanke and Kino.[18] The latter works elaborate on the idea of characterizing the material by two-point correlation of elastic constants, an approach that will be utilized in this work. Also of particular relevance to this article is the work of Bergner *et al.*[19] and Bergner and Köhler,[20] who study the influence of orientation relationships between parent and transformed phases on the attenuation.

The work on backscattering is more recent and less well developed. When single scattering is a valid approximation, one can heuristically think of the backscattering process as one in which the energy scattered by individual crystallites is superimposed at the detector. By assuming that the phases of these signals would be random, Margetan *et al.* developed the independent scattering model, based on the idea that the received power would be equal to the sums of the power[21,22,23,24,25] backscattered from the individual crystallites. This model led to the definition of a characteristic material parameter, which they called figure of merit (FOM), given by the expression $\text{FOM} = n^{1/2}\,\overline{A}$, where n is the number of crystallites per unit volume and $\overline{A}$ is the rms value of the backscattering amplitude of a crystallite in an effective medium.

Despite its conceptual simplicity, this model suffered from two deficiencies: there were no criteria to select the properties of the effective medium and the generalization to multiphased media was not obvious. These difficulties were highlighted by the experimental work of Han et al, which showed that measured backscattered noise is strongly influenced by macrostructure as well as the properties of individual crystallites.[26,27] A foundation to overcome these difficulties was laid by Rose, who developed a formally rigorous stochastic theory for backscattering, based on the assumptions of single scattering and the Born approximation.[28,29,30] This model led Rose to an explicit expression relating the backscattered signals to the microstructure. In particular, he showed that the noise was controlled by the two-point correlation of elastic constant perturbations,

Y.K. HAN, formerly with the Department of Materials Science and Engineering, Iowa State University, is Assistant Manager, Technology Development Department, R&D Center Semiconductor, Samsung Electronics Co., Ltd., San #24 Nongseo-Ri, Kiheung-Eup. Yongin-Goon, Kyungki-Do, Korea. R.B. THOMPSON, Deputy Director, Center for NDE, and Professor, Materials Science and Engineering Department, is with Iowa State University, Ames, IA 50011.

Manuscript submitted June 12, 1995.

$\langle \delta C_{ijkl}(r) \delta C_{pqrs}(r') \rangle$. Here, r and r' are two points in the polycrystal, δC is the local deviation of the elastic stiffness tensor from its Voigt average (C^{VO}) value and $\langle\ \rangle$ denotes an ensemble average. In a single-phased medium, the two-point correlation will be a measure of grain size. When $|r - r'|$ is small with respect to the grain size, there will be a high probability that the two points will fall within the same grain and the correlation will be large. When $|r - r'|$ is large with respect to the grain size, $\delta C(r)$ and $\delta C(r')$ will be uncorrelated and the ensemble average of their product will be small. Using this model, Rose was able to obtain results for randomly oriented, equiaxed, single-phase polycrystals that were identical to those of Margetan *et al.*[2,21–23,25] when the Voigt approximation[31] was used to define the effective medium. He showed that the FOM which Margetan *et al.* defined was identical to the square root of the backscattering coefficient η used by other researchers, particularly in the related field of tissue characterization.

For the two-phase case, due to the complexity of the problem, considerably less work has been done. One of the reasons of the complexity is that the backscattering is caused not only by the acoustic impedance fluctuation of each phase (controlled by grain orientation) but also by the contrast between phases. In the past, most examinations of interphase scattering has been based on the assumption that each phase is macroscopically isotropic, having crystallites whose orientations are random and independent of one another. An example in the weak scattering limit is the work of Rose.[28]

This may be considered a good approach if signals backscattered from phase boundaries are dominant and no orientation relationship is present between phases. However, in advanced materials, often those assumptions are violated depending on processing history, and the consequences may have considerable technological importance. For instance, hard-alpha inclusions in Ti alloys, which have the potential to cause catastrophic aircraft engine failures, have a similar value of acoustic impedance to that of the matrix material. Therefore, backscattering signals from the inclusion-matrix boundaries may be masked by those from acoustic impedance fluctuation in each phase.[2] These backscattered noise signals may be strongly influenced by crystallographic orientation relationships between phases and even between crystallites of a particular phase, resulting in a microstructure with two (or more) dimension scales, which we will term a duplex microstructure. Such conditions are expected to increase the flaw-masking effects of backscattered noise, since any ordered structure generally enhances the intensity of the scattering signals. As detectability of small flaws such as hard-alpha inclusion in Ti alloys becomes more important, these issues also become more significant. Therefore, it is necessary to establish a model that can relate the backscattered signals and these effects.

We thus seek to extend the work of Rose by including the effects of local correlations in the orientations of crystallites. Such situations are found, for example, when the final microstructure is influenced by solid-state transformations in which the final orientation of a particular phase is crystallographically related to that of its parent phase, *e.g.*, microstructures resulting from martensitic or eutectoid transformations. Materials of technological interest in which this occurs include commercial titanium alloys, as noted previously, and pearlitic steels. In this article, we will present the generalization of Rose's theory appropriate to these cases. Our initial developments will be somewhat general and applicable to any material where there is a duplex microstructure in which a parent grain (*e.g.*, a prior beta grain in titanium alloys) is subdivided by solid-state transformation into colonies or crystallites whose orientations are crystallographically related to that of the parent. We will then present a detailed set of numerical results for the case of titanium alloys. These illustrate the angular and frequency dependence of the noise on the ultrasonic wavelength, the sizes of the colonies and parent grains, and the elongation of each. Among the interesting conclusions which can be drawn are the features of the microstructure that control the noise in various frequency regimes.

In Section II, we will briefly review the theory of Rose. This will be followed in Section III by its generalization to the problem previously discussed and in Section IV by the presentation of detailed analytical and numerical results for the case of titanium. Concluding remarks are presented in Section V.

II. GENERAL BACKSCATTERING MODEL

Sigelman and Reid[32] and Madsen *et al.*[33] define the backscattering coefficient $\eta(\omega)$ as the differential scattering cross section per unit volume for a scattering angle of 180 deg, *i.e.*, in the backscattered direction. Here, we will follow that definition and a series of articles by Rose,[28,29,30] elaborating in places on his arguments which only appeared in an abbreviated form as published in a conference proceedings. The central idea is the relationship between the differential scattering cross section and the scattering amplitude, which relates a spherically spreading wave scattered by an inhomogeneity to an incident plane wave. Gubernatis *et al.*[34] present expressions for these scattering amplitudes and differential scattering cross sections for isolated scatterers with constant properties. Consider an incident plane longitudinal wave of the form

$$\mathbf{u} = u^0 \mathbf{e} \exp(ik\mathbf{e}\cdot\mathbf{x}) \qquad [1]$$

where $\mathbf{e}$ is an unit vector in the direction of propagation, $k = \omega/V_l$ is the longitudinal wave propagation constant, and a time dependence of the form $\exp(-i\omega t)$ is assumed. Here, bold characters represent vectors. In the Born approximation and backscattered direction, the scattering amplitude is[28,34]

$$A_i = \frac{e_i}{(4\pi\rho V_l^2)} (\delta\rho\ \omega^2 - \delta C_{jklm}\ k^2 \mathbf{e}_j \mathbf{e}_k \mathbf{e}_l \mathbf{e}_m) \int d^3\mathbf{x} \exp(2ik\mathbf{e}\cdot\mathbf{x}) \qquad [2]$$

where ρ is the density, V_l is the longitudinal wave speed, and $\delta\rho$ and δC are the changes in density and elastic stiffness tensor within the scatterer. Because of the importance of crystallographic orientation in this article, it is necessary to distinguish between elastic constants defined in a coordinate system fixed with a microstructural feature or the sample. Lower-case symbols will be used for the former and upper-case symbols for the latter. Thus, c_{ijkl} are single-crystal elastic constants of a crystallite, c_{ijkl}^{VM} are the Voigt

average elastic constants of a macrograin (averaged over colonies) in the coordinate system of the macrograin, C^{P}_{ijkl} are the elastic constants of a colony in the coordinate system of the sample, C^{M}_{ijkl} are the elastic constants of a macrograin in the coordinate system of the sample, and C_{ijkl} are the elastic constants of the entire sample in its coordinate system.

Within the Born approximation, Eq. [2] may be generalized to a region containing multiple scatterers simply by extending the region of integration to include those scatterers, with $\delta\rho$ and δC being placed in the integrand and interpreted as the differences between the density and elastic stiffnesses of the individual scatterers and the average medium.

Rose has coupled this generalization, the previously given definition of the backscattering coefficient, and the fact that for longitudinal incidence the differential longitudinal wave backscattering cross section is given by $|A^2|$, to arrive at the expression for the backscattering coefficient. Following this procedure, we find

$$\eta = \left(\frac{1}{4\pi\rho V_l^2}\right)^2 \Omega^{-1} \int d^3\mathbf{x} \int d^3\mathbf{x}' \, \langle \omega^2 \delta\rho(\mathbf{x}) - k^2 \delta C_{3333}(\mathbf{x})][\omega^2 \delta\rho(\mathbf{x}') - k^2 \delta C_{3333}(\mathbf{x}')]\rangle \exp\,[2ik(x_3 - x'_3)] \quad [3]$$

where we have assumed the incident wave to propagate in the +3 direction. Here, Ω is the volume of integration, and

$$\delta\rho(\mathbf{x}) = \rho(\mathbf{x}) - \rho^0 \quad [4a]$$

$$\delta C_{3333}(\mathbf{x}) = C_{3333}(\mathbf{x}) - C^0{}_{3333} \quad [4b]$$

where ρ^0 and C^0_{3333} are the spatial averages of the density and elastic stiffness, respectively. The notation $\langle\ \rangle$ denotes an ensemble average over samples with nominally identical microstructures. This result is equivalent to the result that would be obtained by combining Eqs. [7] and [13] of Reference 29, generalized to include the effects of density as well as elastic constant changes, and including a complex conjugation operation that was omitted on the last two sets of fields in Eq. [7] of Reference 29. It should also be noted that Reference 29 established that the backscattering coefficient is equal to the square of the FOM for backscattering, as defined by Margetan and co-workers.[23,24]

The microstructural information enters this theory through quantities of the form $\langle \delta C_{3333}(\mathbf{x})\ \delta C_{3333}(\mathbf{x}')\rangle$, which describe the correlation in the perturbation in properties, in this case of the elastic stiffnesses, at two points in the microstructure. We will use the phrase ''two-point correlation'' to refer to such quantities in the remainder of this article. Other terms in Eq. [3] involve the correlation in the density and the cross correlation of the density and elastic stiffnesses. Rose has discussed how such correlations depend on grain size in equiaxed microstructures involving one[30] or multiple[28] phases with random crystallite orientation. A major purpose of the present article is to extend that work to cases in which the microstructural features may be elongated and have long-range orientation correlations arising from solid-state transformations.

Before proceeding, however, it is convenient to simplify Eq. [3] by a change of variables. The physical motivation is the observation that for macroscopically homogeneous microstructures, the two-point correlation will only depend on the difference, $\mathbf{x} - \mathbf{x}'$. Therefore, if we define the new variables

$$\mathbf{r} = (\mathbf{x} + \mathbf{x}')/2 \quad [5a]$$

$$\mathbf{s} = (\mathbf{x} - \mathbf{x}') \quad [5b]$$

Eq. [3] simplifies to the form

$$\eta = \left(\frac{1}{4\pi\rho V_l^2}\right)^2 \int d^3\mathbf{s} [\omega^4 \langle \delta\rho\delta\rho\rangle(\mathbf{s}) - 2\omega^2 k^2 \langle \delta\rho\delta C_{3333}\rangle(\mathbf{s}) + k^4 \langle \delta C_{3333}\delta C_{3333}\rangle(\mathbf{s})] \exp\,(2iks_3) \quad [6]$$

where notation of the form $\langle\delta\rho\delta\rho\rangle(\mathbf{s})$ represents the quantity $\langle\delta\rho(\mathbf{x})\ \delta\rho(\mathbf{x}')\rangle$, which only depends on $\mathbf{s}$ as noted previously. Here, we have also assumed that $\langle\delta\rho(\mathbf{x})\delta C_{3333}(\mathbf{x}')\rangle = \langle\delta\rho(\mathbf{x}')\delta C_{3333}(\mathbf{x})\rangle$.

Equation [6] provides a general expression for the backscattering coefficient for longitudinal waves, valid in the limit of weak scattering by individual crystallites such that the Born approximation and single-scattering approximations made in this work are valid. An important question regards the range of validity of these approximations. A definitive treatment of these issues goes beyond the scope of this article. However, the following discussion gives some partial insight into this question.

In Reference 29, Rose used the preceding approach to derive an expression for the backscattering coefficient of randomly oriented, equiaxed, single-phase polycrystals. Margetan *et al.*[23,25] have compared Rose's predictions to measurements on well-characterized specimens of copper, stainless steel, and titanium. The results showed, with no adjustable parameters, an absolute agreement between theory and experiment to within a factor of 2, which was taken to be in support of the theory given that the backscattered signals were 40 to 50 dB lower that incident illumination. Rose[28,29,30] also notes that ''the analysis is restricted to that early time portion of the backscattering signal for which acoustic attenuation is negligible.''[28] The essence of his argument is that since each grain represents a weak acoustic contrast, the total wave field is nearly the same as the incident wave field for an early period after the beam enters the solid.[28] In the derivation of the Born approximation for a single scattering, one replaces the actual fields within the scatterer by the incident fields. This is only expected to be a good approximation when the phase difference between these two fields does not become too large. Hence, we hypothesize that sufficient conditions for application of this theory are that the propagation distances involved be such that wave attenuation is small and the microstructural feature size be such that the phase of a wave is not significantly perturbed within the feature from that which it would have in the effective medium.

III. BACKSCATTERING IN DUPLEX MICROSTRUCTURES

A major motivation for this work is the observation that in titanium alloys, there are sometimes large anisotropies in the backscattered noise with no discernible features in

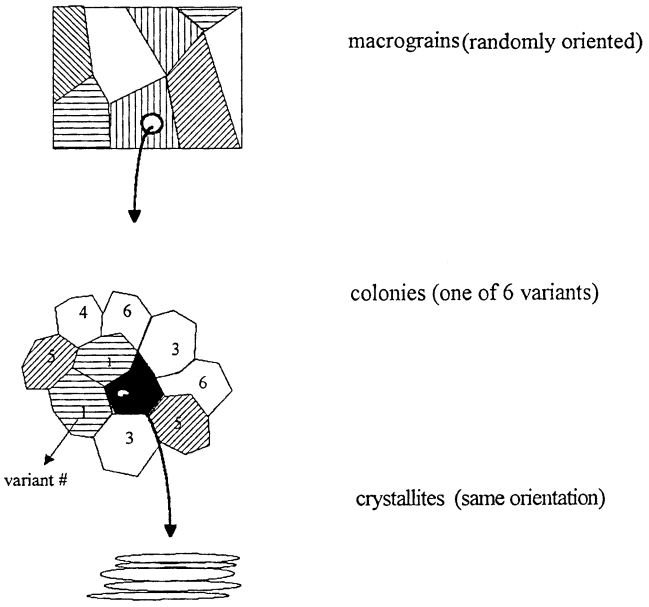

Fig. 1—Different scales of microstructure and their relationship.

optical or SEM micrographs that correlate with this anisotropy.[2,27] Here, we will apply the general backscattering model of the previous section to a set of idealized structures to see if such observations could be explained by correlations in crystallite orientation. Although motivated by titanium alloys, general results will first be derived, valid for any material system in which the microstructure is developed through a solid-state transformation in which the orientation of the transformed phase is restricted to particular values that are related to the orientation of the parent phase. Later, more detailed results will be presented for the particular case of titanium alloys.

There are several microstructural scales in Ti alloys. Figure 1 schematically illustrates a model structure consisting of macrograins, colonies, and crystallites. Such a structure might be developed if a casting were rapidly cooled, such that the beta grains which formed during solidification were converted to transformed beta *via* a martensitic transformation. Because of the crystallographic relationship $(0002)_\alpha // \{110\}_\beta$ and $\langle 11\bar{2}0\rangle_\alpha // \langle 111\rangle_\beta$, the transformed beta would have an orientation given by of one of six elastically distinct variants. Thus, the structure would consist of the three dimension scales shown in Figure 1: macrograins (*i.e.*, prior beta grains), colonies, and crystallites. In the simplified processing sequence described, the macrograins and colonies would be expected to have equiaxed structures with the crystallites being elongated due to the characteristics of martensitic transformation. If this simple process were modified by working in the beta field, one might expect the macrograins to become elongated with the colonies remaining equiaxed. On the other hand, working in the alpha + beta field would produce elongation of both macrograins and colonies.

In commercially important processing sequences, the steps followed and microstructures developed are more complex. However, the preceding structure appears to be simple enough to analyze yet complex enough to contain many elements of reality. Hence, it will be the basis for the analysis in this article.

To simplify the problem further, some additional assumptions are made. First, random orientation of prior beta grains is assumed. In this case, the two-point correlation function for the macrograins will have a simple form. Second, it is assumed that each variant occurs with equal probability. Third, it is assumed that individual crystallites are too small to make a significant contribution to the grain noise. As will be seen based on the analysis of the relative contributions of colonies and prior beta grains, this can be expected to be true when the wavelength is large with respect to the crystallite size. The colonies will be found to have a unique influence on backscattering because they can have only one of six possible orientations within each macrograin. This is quite different from the continuous range of orientations found in single-phase material and will have some interesting and technologically important consequences.

Based on these assumptions, an equation for the two-point correlation function will be evaluated for such a microstructure. Next, a formula for the backscattering coefficient will be derived based on this two-point correlation function. Finally, certain general conclusions regarding the relative importance of macrograins and colonies in determining the backscattering, as inferred from the functional form of the backscattering coefficient, will be discussed. During the development of the theory, a few additional assumptions will be introduced to make the problem simpler, which helps us to understand the factors that control the grain noise in two-phase alloys.

A. *Two-Point Correlation Function*

1. *Randomly oriented, equiaxed, single-phase microstructures*

Consider first a randomly oriented, equiaxed, single-phase polycrystal. Then, the two-point correlation function is controlled by the distribution of grain sizes. If $\mathbf{x}$ and $\mathbf{x}'$ are in different grains, $\delta C(\mathbf{x})$ and $\delta C(\mathbf{x}')$ will be uncorrelated, while if they are in the same grain, they will be highly correlated. For example, Stanke and Kino[18] and Stanke[35,36] have discussed these correlations in detail, including their relationship to standard metallographic definitions of grain size, in the development of theories for ultrasonic attenuation, and Rose[28,29,30] has incorporated similar ideas in his theories for backscattering. As noted by Stanke:[36] ''if the cord lengths have Poisson statistics, then the spatial autocorrelation function has the inverse exponential form.'' Under these conditions, the probability that two points fall within the same grain is described by the function

$$P^G(\mathbf{r} - \mathbf{r}') = \exp\left[-|\mathbf{r} - \mathbf{r}|/a_g\right] \qquad [7]$$

where a_g is the correlation distance, equal to one-half the effective average linear dimensions of the grains.[18] It is this probability function that was employed in the analysis of Rose. Note, however, in the comparison of theory and experiment presented by Margetan *et al.*,[23,25] the experimentally observed form of this function, which differed slightly from an exponential, was utilized.

Under these assumptions, the two-point correlation of the elastic stiffnesses becomes

$$\langle \delta C_{3333}\ \delta C_{3333}\rangle\ (\mathbf{s}) = \langle \delta C^g{}_{3333}\ \delta C^g{}_{3333}\rangle \exp\left[-s/a_g\right] \qquad [8]$$

where the elastic moduli on the right-hand side are the elas-

Table I. Euler Angles for Six Variants with Respect to Cubic Axes of Prior Beta Grain

Euler Angle	Variant 1	Variant 2	Variant 3	Variant 4	Variant 5	Variant 6
ϕ	−45	45	90	90	0	0
θ	−90	−90	−45	45	−45	45
ψ	125.26	125.26	144.74	35.26	144.74	35.26

tic stiffness of a grain and the ensemble average reduces to an average of all orientations of the grain, assumed to be equally probable. The results of this ensemble average have been derived by Rose[29] and are reproduced in the article by Margetan *et al.*[2] This treatment becomes the basis for that of the effects of duplex microstructures.

2. *Duplex microstructures*

To simplify the problem for duplex microstructures, it is assumed that the shapes of macrograins and colonies are independent of their crystallographic orientation and the orientations of the macrograins are random. Based on these assumptions and following the preceding argument, one can relate the two-point correlation of elastic stiffnesses of the sample to that of the macrograin as follows:

$$\langle \delta C_{ijkl}(\mathbf{x}) \delta C_{pqrs}(\mathbf{x}') \rangle = \langle \delta C^{M}_{ijkl}(\mathbf{x}) \delta C^{M}_{pqrs}(\mathbf{x}') \rangle \, P^{M}(\mathbf{x} - \mathbf{x}') \quad [9]$$

where M is a macrograin index, $P^M(\mathbf{x} - \mathbf{x}')$ is a function describing the probability that two points, $\mathbf{x}$ and $\mathbf{x}'$, are in the same macrograin, and $\langle \delta C^M_{ijkl}(\mathbf{x}) \delta C^M_{pqrs}(\mathbf{x}') \rangle$ is the two-point correlation of elastic constants of the points $\mathbf{x}$ and $\mathbf{x}'$ under the condition that they are in the same macrograin. The macrograin two-point correlation function then may be related to the properties of the colonies as follows:

$$\langle \delta C^{M}_{ijkl}(\mathbf{x}) \delta C^{M}_{pqrs}(\mathbf{x}') \rangle = \langle \delta C^{P}_{ijkl} \delta C^{P}_{pqrs} \rangle \, PP(\mathbf{x} - \mathbf{x}') + \sum_{P \neq Q} \langle \delta C^{P}_{ijkl} \delta C^{Q}_{pqrs} \rangle \, PQ(\mathbf{x} - \mathbf{x}') \quad [10]$$

where P and Q are colony indices. The first term treats the case when $\mathbf{x}$ and $\mathbf{x}'$ are in an elastically equivalent variant, which occurs with probability $PP(\mathbf{x} - \mathbf{x}')$. The second term treats the case when the two points are in elastically distinct variants, which occurs with the probability $PQ(\mathbf{x} - \mathbf{x}')$. The quantity $\langle \delta C^P_{ijkl} \delta C^Q_{pqrs} \rangle$ is an ensemble average of the product of the indicated variant elastic moduli, averaged over all macrograin orientations. This would go to zero for large values of $|\mathbf{x} - \mathbf{x}'|$ if the colonies had random orientations. However, if only N elastically distinct variants are allowed, the ensemble averages are finite and $PQ(\mathbf{x} - \mathbf{x}')$ has a limiting value of $(N - 1)^{-1}$.

The ensemble average elastic constant product terms may be obtained by considering the orientation relationship between the sample, the macrograins, and the colonies as follows:

(1) rotate variants P and Q to satisfy crystallographic orientation relationships with respect to macrograin using Euler angles (Table I gives the values appropriate for titanium);
(2) rotate a macrograin with arbitrary set of Euler angles, θ', ϕ', and ψ';
(3) calculate δC^P_{ijkl}, δC^Q_{ijkl}, and $\delta C^P_{ijkl} \delta C^Q_{pqrs}$, and
(4) average over θ', ϕ', and ψ'.

The results, relevant to longitudinal wave backscatter in titanium, obtained using a symbolic manipulation routine in MATHEMATICA are as follows:[37]

$$\langle \delta C^{P}_{3333} \delta C^{P}_{3333} \rangle = (0.975238\ c_{11}^2 - 0.650159\ c_{11}c_{13} + 0.24381\ c_{13}^2 - 1.30032\ c_{11}c_{33} + 0.16254\ c_{13}c_{33} + 0.568889\ c_{33}^2 - 1.30032\ c_{11}c_{44} + 0.975238\ c_{13}c_{44} + 0.325079\ c_{33}c_{44} + 0.975238\ c_{44}^2)/8 \quad [11]$$

where the c_{IJ} are the single-crystal elastic constants of the alpha phase in matrix notation. When $P \neq Q$, there are two cases, depending on whether the parent $\{110\}_\beta$ planes are orthogonal. One finds for orthogonal $\{110\}_\beta$ planes,

$$\langle \delta C^{P}_{3333} \delta C^{Q}_{3333} \rangle = (-0.446984\ c_{11}^2 + 0.16254\ c_{11}c_{13} + 0.0406349\ c_{13}^2 + 0.731429\ c_{11}c_{33} - 0.24381\ c_{13}c_{33} - 0.24381\ c_{33}^2 + 0.325079\ c_{11}c_{44} + 0.16254\ c_{13}c_{44} - 0.487619\ c_{33}c_{44} + 0.16254\ c_{44}^2)/8 \quad [12]$$

and for nonorthogonal $\{110\}_\beta$ planes,

$$\langle \delta C^{P}_{3333} \delta C^{Q}_{3333} \rangle = (-0.129524\ c_{11}^2 + 0.111746\ c_{11}c_{13} - 0.0609524\ c_{13}^2 + 0.147302\ c_{11}c_{33} + 0.0101587\ c_{13}c_{33} - 0.0787302\ c_{33}^2 + 0.223492\ c_{11}c_{44} - 0.24381\ c_{13}c_{44} + 0.0203175\ c_{33}c_{44} - 0.24381\ c_{44}^2)/8 \quad [13]$$

Each variant (P) has one orthogonal and four nonorthogonal pairs (Q), as Figure 2 shows.

Examination of Eq. [6] shows that two-point correlations involving products of densities, and density and elastic constants, are also required in general. However, for the case in hand, in which the contributions of the individual crystallites is neglected, we would expect the average density to be the same in each colony and hence those terms will be neglected in the present work.

For equiaxed macrograins of radius a_m, we will assume that the probability function P^M is the same as that used in prior work, Eq. [7]. Thus, we take

$$P^{M}(\mathbf{s}) = \exp\,[-s/a_m] \quad [14]$$

When the macrograins are elongated, we generalize this to the form used by Ahmed and Thompson[38] in the analysis of attenuation,

$$P^{M}(\mathbf{s}) = \exp\,[-s\{(1 + (a_m^2/c_m^2 - 1)\cos^2(\theta)\}^{1/2}/a_m] \quad [15]$$

Figure 3 shows the geometry of an elongated macrograin, in which the interpretation of c_m as the macrograin radius along the axis of rotational symmetry and a_m as macrograin radius in the perpendicular plane is evident.

Insight into the form of the probability terms $PP(\mathbf{x} - \mathbf{x}')$ and $PQ(\mathbf{x} - \mathbf{x}')$ has been gained from computer simulations of colonies in a macrograin of titanium. In the simulation, an initial macrograin, in the shape of a cube with sides 15-voxels long, was created and divided into cubic voxels whose dimensions were 1/15 of the initial cube. Then, 100 voxels were randomly selected as initial seeds, at which colonies were randomly initiated and assigned one of the six variant orientations. A voxel was then added at a randomly selected position on the boundary of a randomly chosen colony. Here, the unit cube could be added only if

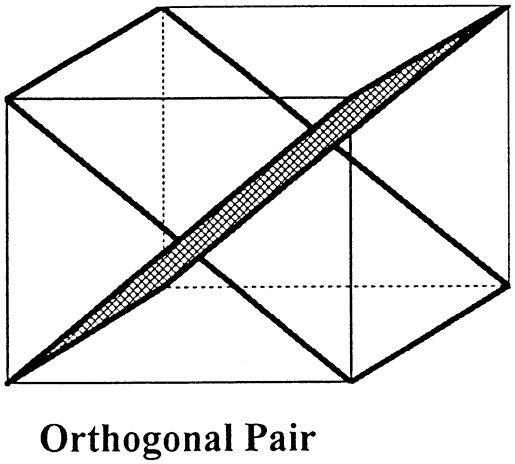

Fig. 2—Schematic representation of relationship between variants (*P* and *Q*).

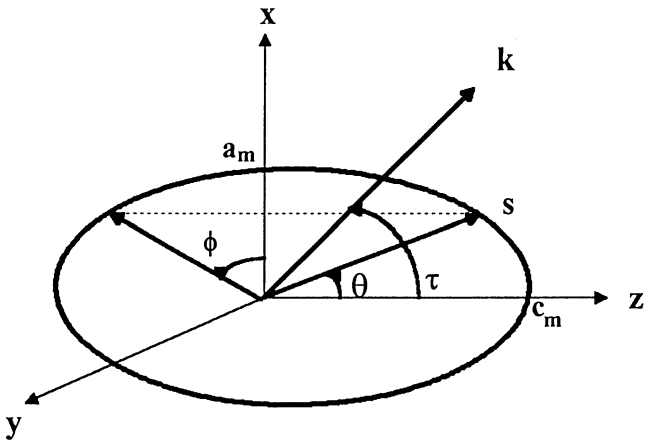

Fig. 3—Schematic representation of elongated macrograin.

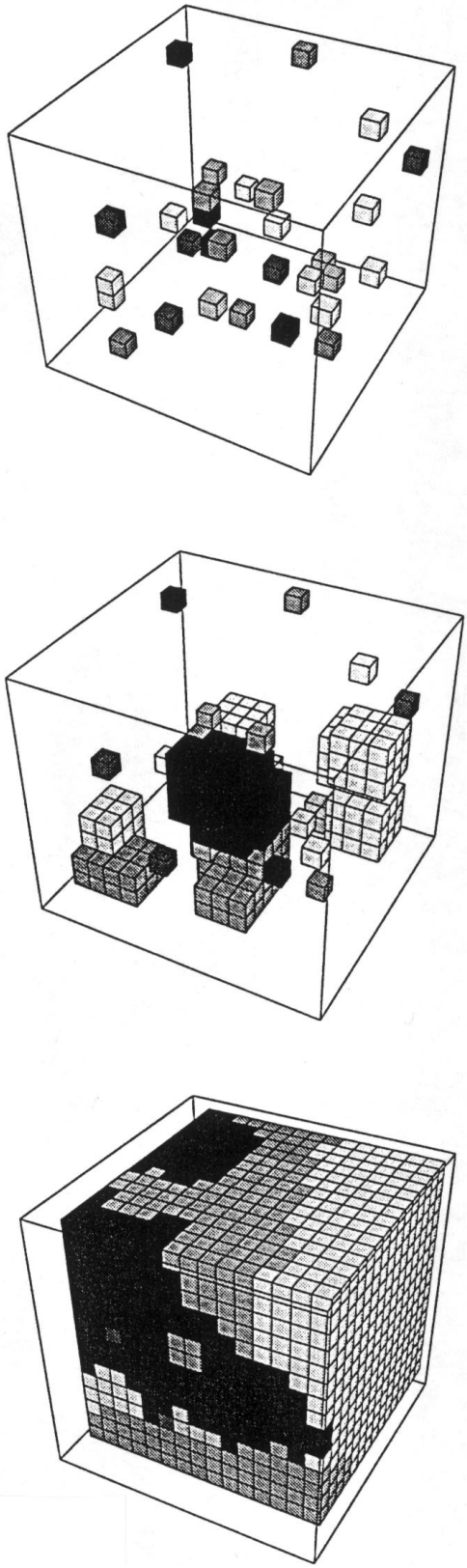

Fig. 4—Schematic representation of simulation of colonies in a macrograin (top: initial seeds; middle: after an interval of growth; and bottom: at the end of growth).

that site was not occupied by other colonies. This growth procedure was repeated until all pixels had been selected and the macrograin was filled with colonies. Figure 4 is a schematic representation of the simulation. After that, two points were randomly picked and checked to determine whether they had the same orientation (variant number) or not. Figure 5 shows $PP(\mathbf{s})$ based on the average result of 40 such simulations. The fact that the results for each variant are essentially identical is consistent with our assumptions.

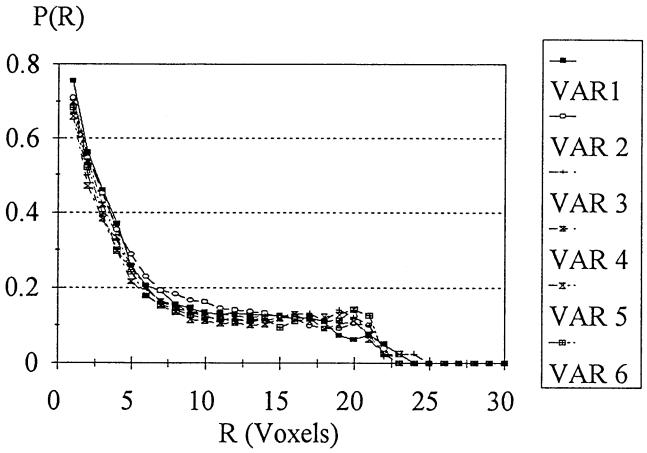

Fig. 5—Probability function, $PP(x - x')$, in two-phase alloy (result of 40 simulations).

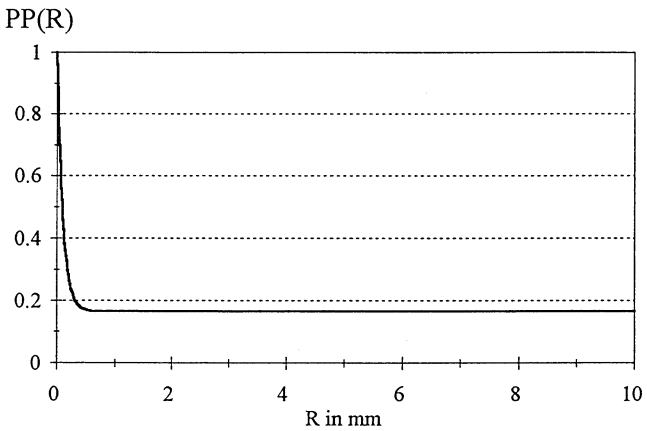

Fig. 6—Probability function, $PP(s)$ (analytical equation), when $a_c = 0.1$ mm.

There are three distinctive regions in Figure 5. In the first region, $PP(\mathbf{x} - \mathbf{x}')$ decreases in a fashion very close to an exponential, which is related to whether the two points are in the same colony or not. This is very similar to the behavior of a single-phase polycrystal. This interpretation is consistent with the fact that the e^{-1} decay constant is approximately $(33.75)^{1/3} = 3.23$ units, where 33.75 is the average volume per grain in cubic units. In the second region, there is a plateau. This is associated with the fact that for largely spaced points, there is always 1/6 probability that the two colonies are of the elastically equivalent variant. In the third region, $PP(\mathbf{x} - \mathbf{x}')$ goes to zero. This is an artifact introduced by the size limit of the simulated macrograin. If the macrograin size were infinite, this cutoff would not exist. Since $PP(\mathbf{x} - \mathbf{x}')$ is only concerned about what happens inside a macrograin, it should not depend on macrograin size. If one of the points is outside the macrograin, P^M goes to zero, so the quantity of $PP(\mathbf{x} - \mathbf{x}')$ is not meaningful anymore. Therefore, it is more reasonable for $PP(\mathbf{x} - \mathbf{x}')$ to approach 1/6 when $|\mathbf{x} - \mathbf{x}'| \to \infty$. Put in other words, this limit is consistent with the fact that $PP(\mathbf{x} - \mathbf{x}')$, as introduced in Eq. [10], is the probability that two points fall in the same variant, assuming that they fall in the same macrograin.

From Figure 5, we see that there are two conditions which $PP(\mathbf{s})$ should satisfy for equiaxed colonies. First, when $\mathbf{s}$ is zero, the function has to be 1. Second, when $\mathbf{s}$ goes to infinity, it should be $1/N$. Considering these conditions, $PP(\mathbf{s})$ is taken to have the following form:

$$PP(\mathbf{s}) = P^C(\mathbf{s}) + [1 - P^C(\mathbf{s})]/N = (N - 1)P^C(\mathbf{s})/N + 1/N \quad [16]$$

where N is the number of elastically distinct variants. (Note that for the beta to alpha transition in titanium, there are 12 variants, but $N = 6$ since the transverse isotropy of the hexagonal alpha phase renders pairs of these elastically indistinguishable.)

Here, we may qualitatively think of P^C as representing the probability that two points are in the same colony. In this work, we will assume $P^C(\mathbf{s})$ to have an exponential form

$$P^C(s) = \exp(-s/a_c) \quad [17]$$

where again a_c is approximately the colony size. Figure 6 shows $PP(\mathbf{s})$ when a_c is 0.1 mm. It will be observed that this function has a shape quite similar to the simulation result shown in Figure 5.

In the case in which the colonies are elongated, we take $P^C(\mathbf{s})$ to have the following form, in analogy to Eq. [15]:

$$P^C(\mathbf{s}) = \exp[-s\{1 + (a_c^2/c_c^2 - 1)\cos^2(\theta)\}^{0.5}/a_c] \quad [18]$$

B. *Figure of Merit*

Using Eqs. [9] and [10], one can relate $\langle \delta C_{ijkl} \delta C_{pqrs} \rangle$ in Eq. [6] to $\langle \delta C^P_{ijkl} \delta C^P_{pqrs} \rangle$, $\langle \delta C^P_{ijkl} \delta C^Q_{pqrs} \rangle$, $P^M(\mathbf{s})$, and $PP(\mathbf{s})$ as follows:

$$\eta = \mathrm{FOM}^2 = \frac{k^4}{(4\pi\rho V_f^2)^2}[\langle \delta C^P{}_{3333} \delta C^P{}_{3333} \rangle \int d^3\mathbf{s} P^M(\mathbf{s})\, PP(\mathbf{s}) \exp(2ik\cdot\mathbf{s}) + (\sum_{P \neq Q} \langle \delta C^P{}_{3333} \delta C^Q{}_{3333} \rangle/(N - 1)) \int d^3\mathbf{s} P^M(\mathbf{s}) \{1 - PP(\mathbf{s})\} \exp(2ik\cdot\mathbf{s})] \quad [19]$$

where $P^M(\mathbf{s})$ and $PP(\mathbf{s})$ are the macrograin probability function and variant probability function previously discussed. Here, we have also assumed

$$PQ(\mathbf{s}) = (1 - PP(\mathbf{s}))/(N - 1) \quad [20]$$

where N is the number of elastically distinct variants ($N = 6$ for Ti).

As mentioned before, macrograins have probability terms similar to equiaxed grains of single-phase material. For equiaxed macrograins, $P^M(\mathbf{s})$ will be assumed to have an exponential form, as Eq. [14] shows.

Substituting Eq. [16] into Eq. [19] and regrouping terms leads to the result

$$\eta = \frac{k^4}{(4\pi\rho V_f^2)^2}[\langle \delta C^M{}_{3333} \delta C^M{}_{3333} \rangle f + \langle \delta C^C{}_{3333} \delta C^C{}_{3333} \rangle g] \quad [21]$$

where

$$f = \int d^3\mathbf{s} P^M(\mathbf{s}) \exp(2ik\cdot\mathbf{s})] \quad [22]$$

$$g = \int d^3\mathbf{s} P^M(\mathbf{s})\, P^C(\mathbf{s}) \exp(2ik\cdot\mathbf{s})] \quad [23]$$

Table II. Elastic Constants of Ti-6Al-4V Annealed Above the Beta Transus and Water Annealed (GPa)

Component		11	12	13	33	44	66
Single crystal (hexagonal)	c_{IJ}	154.24	86.76	63.62	174.45	44.3	33.74
Macrograin Voigt average (cubic)	$c^{VM}{}_{IJ}$	157.293	73.184	73.184	157.293	42.978	42.978
Sample Voigt average (isotropic)	$C^{VO}{}_{IJ}$	158.032	72.814	72.814	158.032	42.609	42.609

$$\langle \delta C^{M}{}_{3333} \delta C^{M}{}_{3333} \rangle = [\langle \delta C^{P}{}_{3333} \delta C^{P}{}_{3333} \rangle + \sum_{P \neq Q} \langle \delta C^{P}{}_{3333} \delta C^{Q}{}_{3333} \rangle]/N \quad [24]$$

$$\langle \delta C^{C}{}_{3333} \delta C^{C}{}_{3333} \rangle = [(N-1)\langle \delta C^{P}{}_{3333} \delta C^{P}{}_{3333} \rangle - \sum_{P \neq Q} \langle \delta C^{P}{}_{3333} \delta C^{Q}{}_{3333} \rangle]/N \quad [25]$$

C. *General Implications*

A number of general conclusions can be drawn from this form. First, consider long wavelengths, *i.e.*, the case of small k. When the colony size becomes sufficiently small, the second term in Eq. [21] will become negligible with respect to the first. One can think of this first term as describing the contributions of the macrograins, had they been viewed as having an average set of elastic constants. The symmetry of these average elastic constants is determined by that of the parent phase, assuming equal populations of each variant. For the case of titanium, this is cubic. Comparing this term to the corresponding result for an aggregate of randomly oriented crystallites having the average elastic stiffness of the macrograins, one finds that the expression for $\langle \delta C^{M}_{3333} \delta C^{M}_{3333} \rangle$ given in Eq. [24] is identical to that which would be obtained for a randomly oriented, single-phase polycrystal if one assumed the average elastic stiffnesses of the macrograin to be given by the Voigt averages[31] of the elastic stiffnesses of all of the variants, c^{VM}_{IJ} (Appendix A). For example, for the case of titanium, in which the average symmetry of the macrograin is cubic, the preceding argument, combined with the results of Rose for single-phased polycrystals,[29] leads to the conclusion

$$\langle \delta C^{M}{}_{3333} \delta C^{M}{}_{3333} \rangle = 48\ (c_{11}{}^{VM} - c_{12}{}^{VM} - 2c^{VM}_{44})^2/1575 \quad [26]$$

In general, one would expect the quantity in parentheses to have a relatively small value, since averaging the elastic stiffnesses of the N anisotropic variants would tend to produce a much more isotropic response. Another consequence of the form of Eq. [21] is the fact that at long wavelength, the backscattering will become independent of direction.

In the opposite limit of high frequency, the second term in Eq. [21] will often become dominant. This may be understood by noting that the integral is essentially a Fourier transform of $P^M(\mathbf{s})P^C(\mathbf{s})$. Since this function can be much more localized than $P^M(\mathbf{s})$, which appears in the integral of the first term, higher values will be expected at large k. From the physical perspective, this is a consequence of the fact that the scattering is dominated by the structure whose scale is on the order of the wavelength, in this case, the colonies. The relative values of the coefficients, $\langle \delta C^{M}_{3333} \delta C^{M}_{3333} \rangle$ and $\langle \delta C^{C}_{3333} \delta C^{C}_{3333} \rangle$ will influence when the crossover from macrograin to colony response occurs. In general, one would expect $\langle \delta C^{C}_{3333} \delta C^{C}_{3333} \rangle$ to be considerably greater, since it is approximately equal to $\langle \delta C^{P}_{3333} \delta C^{P}_{3333} \rangle$, controlled by the anisotropic stiffness of the colony rather than the macrograin.

IV. RESULTS FOR PARTICULAR MACROGRAIN AND COLONY GEOMETRIES IN TITANIUM

If P^M and P^C are provided, the FOM may be calculated. In this section, such a calculation will be performed for a variety of cases involving spherical or elongated macrograins and colonies. The elastic constants are estimated values selected to correspond to the case of a sample of titanium annealed above the beta transus (the boundary in the phase diagram which separates the high-temperature β phase and the low-temperature α phase) followed by quenching. It is assumed that all of the β phase transforms to α' of the same concentration. The numerical values appear in Table II.[37]

Before presenting these results, however, some further comments are required regarding accuracy, although as noted in Section II, these must be viewed as somewhat speculative. The foundation of the discussion is the previously reported comparison between theory and experiment, which showed that our basic assumptions, single scattering and the Born approximation, are valid for early time arrivals in randomly oriented polycrystals of copper, stainless steel, and alpha titanium. In those measurements, ka ranged from 0.3 to 0.7. It would therefore seem to be a reasonable approximation that our approaches are useful at early times when $ka \lesssim 1$ for such materials, with the accuracy at larger values an open question.

As an independent check on this notion, consider the Born approximation. There, it is assumed that we can replace the true wavefield by the incident wavefield within the scattering object. The degree to which this is possible will depend on the anisotropy of the material. For the elastic moduli of alpha titanium given in the first row Table II, the ratio of the speeds of longitudinal waves traveling in the ''3'' and ''1'' directions is 1.06 ($\sqrt{c_{33}/c_{11}}$). With respect to the velocity computed from the sample Voigt average ($\sqrt{[8c_{11} + 3c_{33} + 4c_{13} + 8c_{44}]/15\rho}$), the speed is greater by 5.1 pct in the 3-direction and lower by 1.2 pct in the 1–2 plane. Taking the former as a worst case, the error in phase between a wave propagating in the effective medium and in the anisotropic grain along the 3-direction is $\Delta\phi = 0.1$ radian $= 5.7$ deg when $ka = 1$. In other directions, it is less. This seems to be a reasonable regime in which to apply the Born approximation. Based on both the compar-

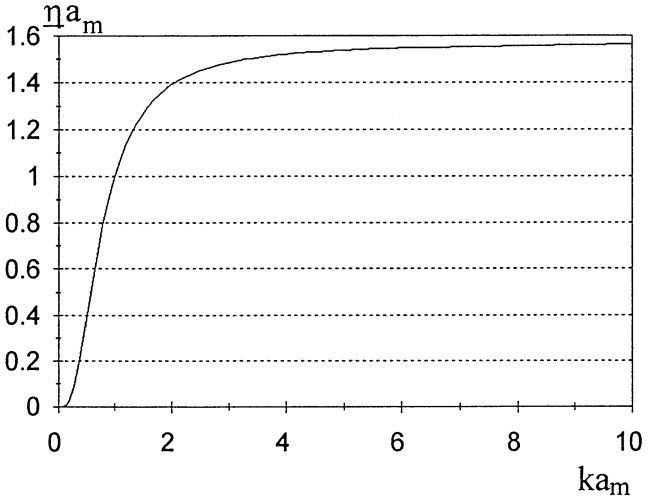

Fig. 7—$\underline{\eta}a_m$ *vs* ka_m for equiaxed macrograins ignoring colonies.

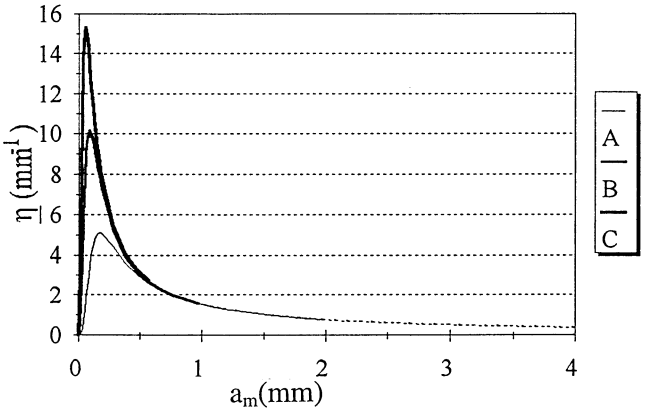

Fig. 8—$\underline{\eta}$ *vs* a_m for equiaxed macrograins ignoring colonies (*A*: $k = 5$ mm^{-1}; *B*: $k = 10$ mm^{-1}; and *C*: $k = 15$ mm^{-1}).

ison of theory and experiment discussed in the previous paragraph and the theoretical arguments given previously, a reasonable criteria for convergence would appear to be $ka_c \leq 1$, where a_c is the radius of the colony in the direction of propagation.

The macrograins can be considerably larger. However, because their average stiffnesses are considerably less anisotropic in our model because of the equal probability given to all variants, the Born approximation may still be appropriate. For the cubic symmetry of the average elastic constants of the macrograins, the wave speeds in the [100], [110], and [111] directions are $\sqrt{c_{11}^{VM}/\rho}$, $\sqrt{(c_{11}^{VM} + c_{12}^{VM} + 2c_{44}^{VM})/2\rho}$, and $\sqrt{(c_{11}^{VM} + 2c_{12}^{VM} + 4c_{44}^{VM})/3\rho}$. These are, respectively, 0.23 pct lower, 0.06 pct higher, and 0.15 pct higher than the sample Voigt average. Taking the [111] direction as the worst case, it is reasonable to assume that the maximum macrograin size scales with respect to the maximum colony size as the inverse of their anisotropy. Thus, we would expect reasonable predictions up to at least $ka_m = 10$.

In the numerical results that follow, we will show predictions within the preceding ranges ($ka_c \leq 1$, $ka_m \leq 10$) as solid lines. When colonies or macrograins are not spherical, the dimension parallel to the direction of propagation will be used. Since these arguments, ultimately based on the aforementioned comparison to experiment for equiaxed polycrystals, set lower bounds, the curves will be extended as dashed lines to indicate their greater uncertainty. At present, we have no quantitative estimate of the uncertainties of the model predictions in this regime.

A. *Macrograins Ignoring Colony Effect*

We first consider the case in which the size of the colonies is sufficiently small that the macrograin can be viewed as a continuum. As was discussed previously, for the case of titanium and our idealized assumptions, this macrograin will have cubic symmetry. We will separately treat the cases of equiaxed and elongated macrograins.

1. *Spherical macrograins ignoring discreteness of colonies*

Inserting Eqs. [14], [17], and [22] through [25] into Eq. [21] and evaluating the integral, the following equation is obtained in the limit $a_c \rightarrow 0$:

$$\eta = \frac{k^4}{(4\pi\rho V_l^2)^2} \langle \delta C^M{}_{3333} \delta C^M{}_{3333} \rangle \, [8\pi a_m{}^3/(1 + 4k^2 a_m{}^2)^2] \quad [27]$$

As noted in section III.C, this result is the same as that previously derived for the single-phase case. We find it convenient to define the normalized quantity $\underline{\eta} = (4\pi\rho V_l^2)^2 \eta / \langle \delta C^M_{3333} \delta C^M_{3333} \rangle$. Then $\underline{\eta}$ is given by

$$\underline{\eta} = 8\pi a_m{}^3 k^4/(1 + 4k^2 a_m{}^2)^2 \quad [28]$$

which eliminates the effects of the macrograin elastic constants. In the absence of colonies, $\underline{\eta}$ illustrates the dependence of backscatter on macrograin size and frequency and has the dimension of length^{-1}. Figure 7 shows the behavior of the dimensionless quantity $\underline{\eta}a_m$ as a function of ka_m. As noted previously by Rose, in the low-frequency region ($ka_m << 1$), $\underline{\eta}a_m$ is proportional to k^4 (Rayleigh region), and in the high-frequency region ($ka_m >> 1$), it becomes constant ($\pi/2$).

Figure 8 presents a series of plots showing how $\underline{\eta}$ depends on a_m at different values of k. By fixing k, we can see that $\underline{\eta}$ increases at low a_m, reaches a maximum, and then decreases, approaching zero as a_m approaches infinity. The value of $\underline{\eta}$ is maximum at $a_m = \sqrt{3}/(2k)$. The physical interpretation of this result is that the backscattering will first increase as macrograin size increases and the medium becomes less like a continuum. However, a maximum must be reached because as macrograin size continues to grow, the medium becomes more like a single crystal, which has no backscattering.

In this and subsequent plots of $\underline{\eta}$ *vs* k, it may be of interest to note that the frequency f is equal to $V_l k/2\pi$. Since $V_l \sim 2\pi$ in units of mm/μs for titanium and a number of other common metals, the numerical k in mm^{-1} is close to the numerical value of f in MHz for such materials. Hence, these plots also can be interpreted in terms of typical ultrasonic frequencies. For example, use of such relations says that at 5 MHz, the maximum, macrograin-only backscattering would be for the values of $a_m \sim 0.17$ mm.

2. *Elongated Macrograins Ignoring Discreteness of Colonies*

Next, the effects of macrograin shape will be discussed. In this case, we assume that $P^M(\mathbf{s})$ is now described by Eq.

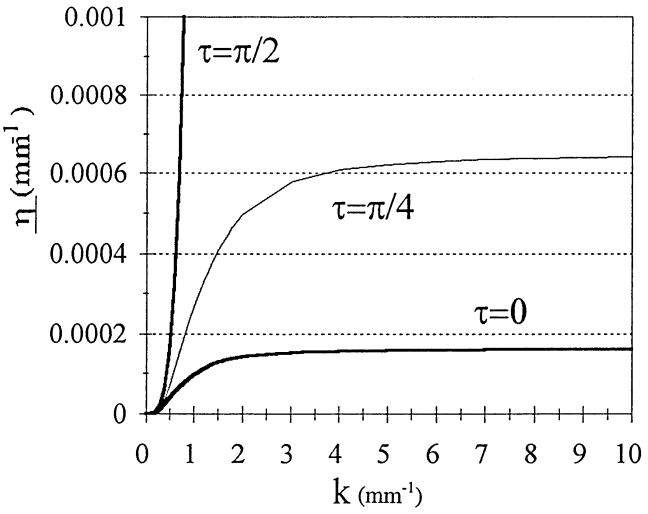

Fig. 9—$\underline{\eta}$ *vs* k ignoring colonies (a_m = 0.01 mm and c_m = 1 mm).

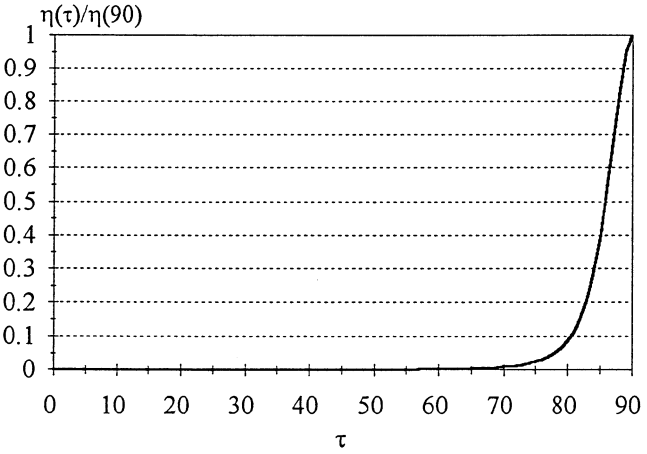

Fig. 10—$\eta(\tau)/\eta(90\text{ deg})$ *vs* τ ignoring colonies (k = 5 mm^{-1}; a_m/c_m = 0.01; and c_m = 1 mm).

[15], which was schematically illustrated in Figure 3. Based on this geometry and Eq. [21], the normalized backscattering coefficient becomes

$$\underline{\eta} = k^4 \iiint ds d\theta d\phi\, s^2 \sin(\theta)\, P^M(\mathbf{s}) \exp[2iks \{\sin(\theta)\sin(\tau)\sin(\phi) + \cos(\theta)\cos(\tau)\}] \quad [29]$$

where τ is the angle of propagation with respect to the major axis of the elongated macrograin. In this case, the normalized backscattering coefficient becomes

$$\underline{\eta} = k^4 \int_0^{2\pi}\int_0^{\pi}\int_0^{\infty} \exp(-As)\, s^2 \sin(\theta)\, ds\, d\theta\, d\phi \quad [30a]$$

$$= k^4 a_m{}^3 \int_0^{2\pi}\int_0^{\pi} 2\sin(\theta)/(A\, a_m)^3\, d\theta\, d\phi \quad [30b]$$

where

$$A = \{1 + (a_m{}^2/c_m{}^2 - 1)\cos^2(\theta)\}^{0.5}/a_m + 2ik\{\sin(\theta)\sin(\tau)\sin(\phi) + \cos(\theta)\cos(\tau)\} \quad [31]$$

An analytical expression for the angular integral has not been available. Therefore, numerical integration using a subroutine used in Reference 38 was performed to obtain the following figures. The result of the numerical integration yielded a well-behaved function with zero imaginary part, as would be expected on physical grounds.

Figure 9 presents a series of plots of $\underline{\eta}$ against k for three different values of τ (direction of propagation with respect to orientation of macrograin) for a macrograin having a 100:1 aspect ratio and a value of c_m = 1. It is interesting to note that at low frequencies, the backscattering is isotropic, while at high frequencies, the backscattering is greatest for illumination perpendicular to the long axis of macrograin. Figure 10 shows $\eta(\tau)/\eta(90\text{ deg})$ *vs* τ at k = 5 mm^{-1} for the same microstructure. One would expect that at short λ (high k), local curvature (evaluated at the point at which the incident wavefront becomes tangent to an ellipse having the aspect ratio of the macrograin) is a dominant factor (the higher the radius curvature, the higher the backscattering coefficient). For instance, for the spherical macrograin case, $\underline{\eta}$ was proportional to $\pi/2a_m$ in the high-frequency region. The local radius of curvature increases as τ increases. Therefore, the η should also increases as τ increases, as shown in Figure 10. On the other hand, at long λ, examination of Eq. [21] shows that $\underline{\eta} = k^4 V_e$, where $V_e = \int d^3\mathbf{s} P^M(\mathbf{s})$. Figure 9 confirms such behavior. In summary, η behaves differently as a function of τ, depending on the value of k. The effect of elongation is more prominent at higher frequency.

B. *Macrograins Considering Discreteness of Colonies*

1. *Spherical macrograins with spherical colonies*

In this case, η can be evaluated using Eqs. [14], [17], and [21] through [25]. The latter may be rewritten as follows:

$$\eta = \frac{k^4}{(4\pi\rho V_l^2)^2}\left[\langle \delta C^M{}_{3333}\delta C^M{}_{3333}\rangle f_1 + \langle \delta C^C{}_{3333}\delta C^C{}_{3333}\rangle g_l\right] \quad [32]$$

where

$$f_l = 8\pi a_m{}^3/(1 + (2a_m k)^2)^2 \quad [33]$$

$$g_l = 8\pi\{a_m a_c/(a_m + a_c)\}^3/[1 + \{2ka_m a_c/(a_m + a_c)\}^2]^2 \quad [34]$$

Equation [32] clearly separates the contributions of the macrograins and colonies. Based on Eqs. [32] through [34], the dependence of $\underline{\eta}$ on k has been examined. Figure 11(a) compares the responses for size ratios (a_c/a_m) of 0.1, 0.01, 0.001, and 0, consistent with previous discussions. Considering the macrograin only response (a_c/a_m = 0, case A) as a reference, one sees that the effect of the colonies is to cause deviation from the macrograin-only case, occurring at lower frequencies as the colony size increases. This is reasonable behavior because colonies are a smaller scale microstructural feature, so their effect should be more significant in the higher frequency (shorter wavelength) region.

Other aspects of the relative contributions of colonies and macrograins are illustrated in Figure 11(b), in which the same information has been slotted in a different frequency regime to highlight the contributions of the colonies. Here, $\underline{\eta}$ is plotted *vs* k for much larger values of k with a_c/a_m as a parameter and a_m = 1 mm. These are the same cases that

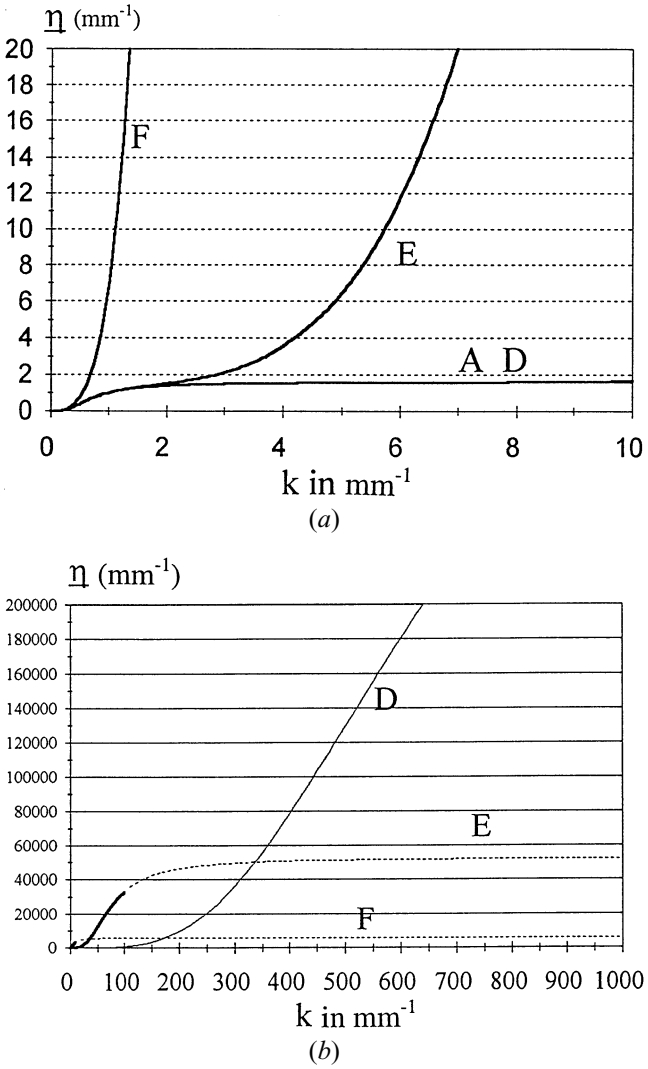

Fig. 11—$\underline{\eta}$ *vs* k for equiaxed macrograin and colonies with a_m = 1 mm (A: macrograin only; D: a_c/a_m = 0.001; E: a_c/a_m = 0.01; and F: a_c/a_m = 0.1) (*a*) at low k regime and (*b*) at high k regime.

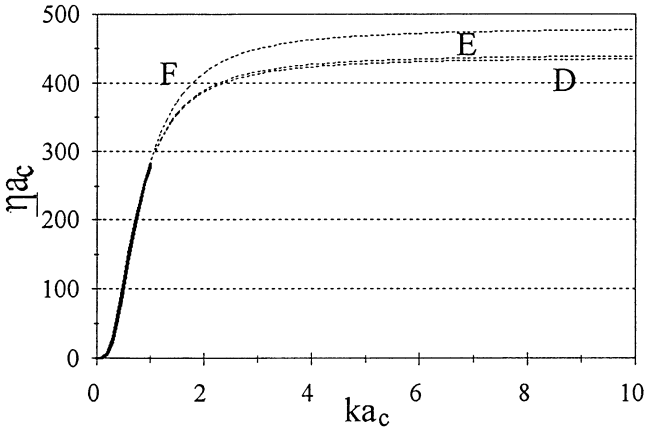

Fig. 12—$a_c\underline{\eta}$ *vs* ka_c for equiaxed macrograin and colony with a_m = 1 mm (D: a_c/a_m = 0.001; E: a_c/a_m = 0.01; and F: a_c/a_m = 0.1).

were shown in Figure 11(a), but the macrograin-only response has been omitted since it would be indistinguishable from the abscissa. It can be seen that as one decreases the colony size, the backscattering starts to grow at a higher frequency but approaches a higher plateau. The former is a consequence of the requirement that $ka_c \sim 1$ for significant interaction. The latter is a consequence of the fact the number of colony boundaries per unit volume, which individually scatter energy, varies as a_c^{-3}. However, one requires $ka_c >> 1$ before the scattering from individual boundaries is fully effective.

In regimes in which the colonies dominate the scattering, it might be more illuminating to examine a dimensionless plot, which was normalized by a_c rather than a_m. Such a case is shown in Figure 12. One can see that the complex behavior shown in Figure 11(b) can be explained in a unified way by such a plot. The high-frequency asymptotic limit is as follows:

$$\underline{\eta} a_c = \pi\left[\frac{\langle \delta C^C_{3333} \delta C^C_{3333} \rangle}{\langle \delta C^M_{3333} \delta C^M_{3333} \rangle} \left(\frac{a_m + a_c}{2a_m}\right)\right] \qquad [35]$$

The fact that $\langle \delta C^C_{3333}\ \delta C^C_{3333} \rangle / \langle \delta C^M_{3333} \delta C^M_{3333} \rangle >> 1$ is the reason the plateau in Figure 12 is much higher than that in Figure 7. The underlying physical reason is that the anisotropy of the elastic stiffnesses of the colonies is much greater than that of the Voigt average of the variants in the macrograin.

2. *Elongated macrograins with equiaxed colonies*

So far, it has been shown that colonies affect the backscattering significantly, especially in the high k region. Therefore, it is suspected that colonies would result in interesting behaviors when they are elongated. Depending on processing history, the colonies may be equiaxed or elongated. If colonies were formed before deformation of macrograins, then colonies would be elongated. On the other hand, if they were formed after the deformation of macrograins, they might be equiaxed. The latter case was considered first.

Inserting Eqs. [15] and [17] into [21], the resulting equation for FOM is as follows:

$$\eta = \frac{k^4}{(4\pi\rho V_{\bar{l}}^2)^2} [\langle \delta C^M{}_{3333} \delta C^M{}_{3333} \rangle f_2 + \langle \delta C^C{}_{3333} \delta C^C{}_{3333} \rangle g_2] \qquad [36]$$

where

$$f_2 = \int d^3s \exp\left[-s\{1 + (a_m^2/c_m^2 - 1)\cos^2(\theta)\}^{0.5}/a_m\right] \exp\left[2iks\{\sin(\theta)\sin(\tau)\sin(\phi) + \cos(\theta)\cos(\tau)\}\right] \qquad [37]$$

$$g_2 = \int d^3s \exp\left[-s\{1 + (a_m^2/c_m^2 - 1)\cos^2(\theta)\}^{0.5}/a_m\right] \exp\left[-s/a_c\right] \exp\left[2iks\{\sin(\theta)\sin(\tau)\sin(\phi) + \cos(\theta)\cos(\tau)\}\right] \qquad [38]$$

Here, f_2 is the same function that appeared in Eqs. [29] and [30]. The g_2 has a similar form to Eq. [30a], except A has been replaced by A_2, where

$$A_2 = \{1 + (a_m^2/c_m^2 - 1)\cos^2(\theta)\}^{0.5}/a_m + 2ik\{\sin(\theta)\sin(\tau)\sin(\phi) + \cos(\theta)\cos(\tau)\} + 1/a_c \qquad [39]$$

Therefore, the same numerical analysis techniques which were used to evaluate Eq. [32] were applied in this case, too.

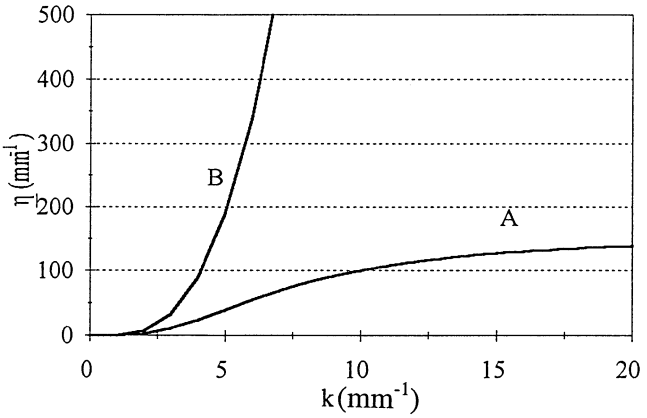

Fig. 13—$\underline{\eta}$ *vs* k for elongated macrograin with equiaxed colonies with c_m = 1 mm, a_m/c_m = 0.1, a_c/a_m = 0.5, and $\tau = \pi/2$ (A: macrograin only and B: macrograin with colonies).

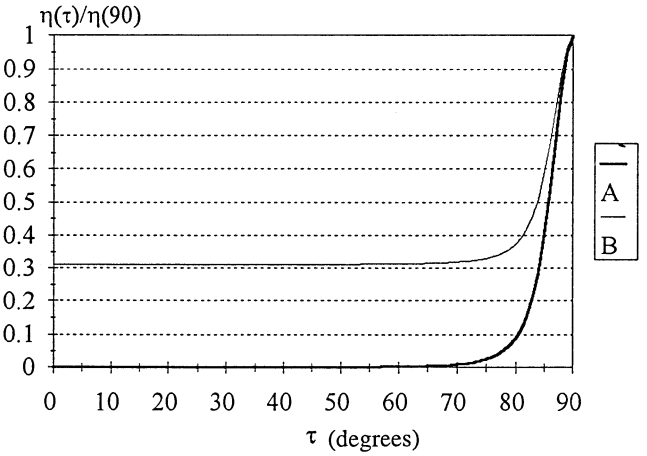

Fig. 14—$\eta(\tau)/\eta$ (90 deg) *vs* τ. When k = 10 mm^{-1}, a_m/c_m = 0.1, c_c/a_m = 0.1, c_c/a_c = 1, and c_m = 1 mm (A: macrograin only and B: considering the colony effect).

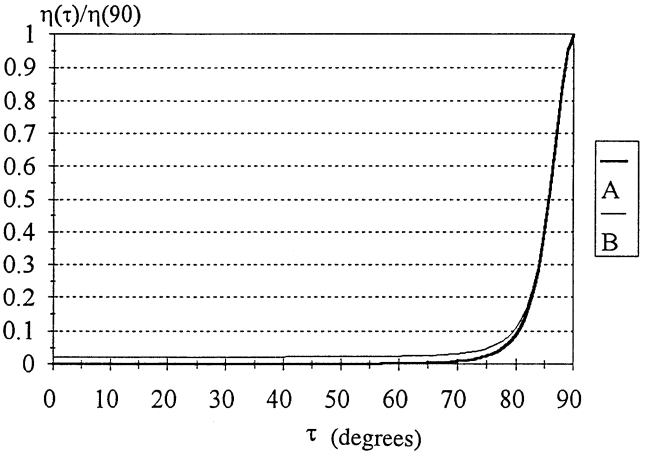

Fig. 15—$\eta(\tau)/\eta$ (90 deg) *vs* τ. When k = 10 mm^{-1}, a_m/c_m = 0.1, c_c/a_m = 0.1, c_c/a_c = 0.2, and c_m = 1 mm (A: macrograin only and B: considering colony effect).

Figure 13 shows the effect of colonies on the frequency dependence of backscattering when c_m = 1 mm, a_m/c_m = 0.01, a_c/a_m = 0.1, and $\tau = \pi/2$. The increasing contribution of the colonies at higher frequencies is clearly demonstrated. It is interesting that the colony effect becomes noticeable at surprisingly low values of ka_c (~0.01). We speculate that this is related to the much greater elastic anisotropy of the colonies with respect to the macrograins. A similar behavior has been shown in Figure 11(a).

Figure 14 compares the angular dependence of $\eta(\tau)/\eta$(90 deg) for the cases when colonies are ignored and considered. It was previously shown that for macrograins only, η reaches a higher asymptotic limit when the radius of curvature in that direction is higher. However, η shows a much more isotropic behavior when the colonies are considered. The reason is that the colonies are equiaxed. As mentioned before, the colony effect will be more dominant in the high k region. Therefore, as k increases, η will be more isotropic. We also have seen that backscattering is isotropic at long wavelength, a result that can be reconfirmed by examining the limits of Eqs. [37] and [38] as k goes to 0. Hence, for this case, there must be some intermediate frequency at which the anisotropy is greatest.

3. *Elongated macrograins and elongated colonies*

Equation [36] may be used in this case, too, if g_2 is replaced by the following g_3:

$$g_3 = \int d^3s \exp\left[-s\left\{1 + (a_c^2/c_c^2 - 1)\cos^2(\theta)\right\}^{0.5}/a_c\right] \exp\left[-s\left\{1 + (a_m^2/c_m^2 - 1)\cos^2(\theta)\right\}^{0.5}/a_m\right] \exp\left[2iks\left\{\sin(\theta)\sin(\tau)\sin(\phi) + \cos(\theta)\cos(\tau)\right\}\right] \quad [40]$$

The preceding g_3 also may be evaluated using Eq. [30a] if A is replaced by following A_3:

$$A_3 = \left\{1 + (a_m^2/c_m^2 - 1)\cos^2(\theta)\right\}^{0.5}/a_m + 2ik\left\{\sin(\theta)\sin(\tau)\sin(\phi) + \cos(\theta)\cos(\tau)\right\} + \left\{1 + (a_c^2/c_c^2 - 1)\cos^2(\theta)\right\}^{0.5}/a_c \quad [41]$$

Here, the $\underline{\eta}$ behaves similarly to the former case; when $ka_c << 1$, colonies are ignorable, but at $ka_c >> 1$, colonies are dominant. However, since colonies are elongated in this case, the η shows a significant angular dependence, regardless of whether the colonies are considered, as Figure 15 shows. The anisotropy is less in the presence of colonies because of their smaller ellipticity. Again, at sufficiently long wavelength, the response must become isotropic.

V. SUMMARY

A theory has been presented that predicts the backscattering coefficient in duplex microstructures consisting of macrograins containing colonies whose orientations are crystallographically related and assumed to occur with equal probability. Included is a qualitative discussion of the expected accuracy of the major assumption: single scattering treated by the Born approximation. The results are presented in general form and then specified to the case of microstructure characteristics of titanium alloys.

The main difference between the alloys of duplex microstructures and single-phase alloys is the presence of colonies with specific crystallographic relationships to the parent grain (prior beta in the case of titanium). It has been found that these differences have several important consequences on the theory of backscattering. First, these crystallographic relationships result in nonzero values of the quantity $\langle \delta C^P_{ijkl} \delta C^Q_{pqrs} \rangle$ when P is not equal to Q. Second,

because of the finite number of variants, there is always a finite probability that two points in the same macrograin will lie in the same variant, no matter how far apart they are as compared to the colony size. Consequently, a plateau region exists when one plots the two-point correlation of elastic stiffnesses *vs* separation of two points in a macrograin. The backscattering coefficient (η) was calculated based on these effects. For sufficiently small colonies, the results are found to be equivalent to those obtained when the macrograins are viewed as a homogeneous continuum whose properties can be taken as a Voigt average of those of the variants. However, finite colonies can make significant additional contributions to the backscattered noise when the wavelength approaches their size. Thus, the backscattering depends on the microstructure in a complex way that is controlled by the relative values of ultrasonic frequency, macrograin size and shape and colony size and shape. At sufficiently long wavelengths, the backscattering is found to be isotropic. At wavelengths approaching the colony size, the anisotropy of the backscattering will be controlled by the colony elongation. At intermediate wavelengths, the anisotropy of the backscattering is a complex function of the elongation of the macrograins and colonies.

ACKNOWLEDGMENT

This material is based upon work performed at the FAA Center for Aviation Systems Reliability operated by Iowa State University and supported by the Federal Aviation Administration under Grant No. 93-G-018. Any opinions, findings, conclusions, or recommendations expressed in this material are those of the authors and do not necessarily reflect the views of the Federal Aviation Administration.

APPENDIX A
Equivalence of duplex analysis, in the limit of small colonies, to results of a continuum model of macrograins

In the Voigt approximation, the continuum elastic stiffnesses of a macrograin are given by

$$c_{ijkl}^{VM} = \frac{1}{N}\sum_{P=1}^{N} c_{ijkl}^{PM} \qquad [A1]$$

where c_{ijkl}^{PM} are the colony elastic stiffnesses of variant P, also expressed in the coordinate system of the macrograin. In the coordinate system of the sample, this takes the form

$$C_{ijkl}^{VM} = \frac{1}{N}\sum_{P=1}^{N} C_{ijkl}^{P} \qquad [A2]$$

where lower cases have been changed to upper cases to denote the changes in coordinates. The Voigt average stiffnesses of the sample are then

$$C_{ijkl}^{VO} = \langle C_{ijkl}^{VM}\rangle = \langle C_{ijkl}^{P}\rangle \qquad [A3]$$

Viewing the macrograin as the fundamental microstructural unit (*i.e.*, ignoring the individual colonies and viewing the macrograin as a continuum) and following the analysis of Rose,[29] we know that the backscattered noise is controlled by the quantity $\langle \delta C_{3333}^{VM} \delta C_{3333}^{VM}\rangle$, where

$$\delta C_{ijkl}^{VM} = C_{ijkl}^{VM} - C_{ijkl}^{VO} \qquad [A4]$$

Simple arithmetic then shows that

$$\langle \delta C_{3333}^{VM} \delta C_{3333}^{VM}\rangle = \langle (C_{3333}^{VM} - C_{3333}^{VO})(C_{3333}^{VM} - C_{3333}^{VO})\rangle$$
$$= \langle (\frac{1}{N}\sum_{P=1}^{N} C_{3333}^{P} - \langle C_{3333}^{P}\rangle)(\frac{1}{N}\sum_{Q=1}^{N} C_{3333}^{Q} - \langle C_{3333}^{Q}\rangle)\rangle \qquad [A5]$$
$$= \frac{1}{N^2}\langle (\sum_{P=1}^{N} \delta C_{3333}^{P})(\sum_{Q=1}^{N} \delta C_{3333}^{Q})\rangle = \frac{1}{N}\langle \delta C_{3333}^{P} \sum_{Q=1}^{N} \delta C_{3333}^{Q}\rangle$$

for any P, where

$$\delta C_{3333}^{P} = C_{3333}^{P} - C_{3333}^{VO} \qquad [A6]$$

The left-hand side of Eq. [A5] controls the noise in the single-phase analysis, as is indicated in Eq. [26]. The right-hand side of Eq. [A5] is equivalent to Eq. [24] and thus is the quantity that controls the noise in the current duplex analysis when the colonies are small. Hence, the analyses are equivalent in this limit, as would be expected.

REFERENCES

1. K. Goebbles: *Research Techniques in Nondestructive Testing*, Academic Press, New York, NY, 1980, pp. 87-157.
2. F.J. Margetan, R.B. Thompson, I.Y. Yalda, and K.Y. Han: *Detectability of Small Flaws in Advanced Engine Alloys*, Iowa State University, Ames, IA, 1993.
3. B.R. Tittmann and L. Ahlberg: *Review of Progress in Quantitative NDE*, Plenum Press, New York, NY, 1983, vol. 2A, pp. 129-45.
4. I.M. Lifshits and G.D. Parkhomovskii: *Uc. Zap. Charkov Cos. Univ. Im.*, 1948, vol. 27, pp. 25-35.
5. I.M. Lifshits and G.D. Parkhomovskii: *Zh. Eksp. Theor. Fiz.*, 1950, vol. 20, pp. 175-82.
6. A.B. Bhatia: *J. Acoust. Soc. Am.*, 1959, vol. 31, pp. 16-20.
7. A.B. Bhatia: *Ultrasonic Absorption*, Clarendon Press, Oxford, United Kingdom, 1967.
8. A.B. Bhatia and R.A. Moore: *J. Acoust. Soc. Am.*, 1959, vol. 31, pp. 1140-41.
9. L.L. Rokhlin: *Sov. Phys. Acoust.*, 1972, vol. 18, pp. 71-75.
10. R. Truell, C. Elbaum, and B.B. Chick: *Ultrasonic Methods in Solid State Physics*, Academic Press, New York, NY, 1969.
11. P.C. Waterman and A. Truell: *J. Math. Phys.*, 1961, vol. 2, pp. 512-37.
12. E.P. Papadakis: *Physical Acoustics*, Academic Press, New York, NY, 1968, vol. 6B, pp. 278-309.
13. S. Hirsekorn: *J. Acoust. Soc. Am.*, 1982, vol. 72, p. 1021.
14. S. Hirsekorn: *J. Acoust. Soc. Am.*, 1983, vol. 73, p. 1160.
15. S. Hirsekorn: *J. Acoust. Soc. Am.*, 1985, vol. 77, p. 832.
16. S. Hirsekorn: *J. Acoust. Soc. Am.*, 1986, vol. 79, p. 1269.
17. S. Hirsekorn: *J. Acoust. Soc. Am.*, 1988, vol. 83, p. 1231.
18. F.E. Stanke and G.S. Kino: *J. Acoust. Soc. Am.*, 1984, vol. 75, p. 665.
19. F. Bergner, B. Köhler, and K. Popp: *Int. J. Pres. Ves. Piping*, 1993, vol. 55, pp. 251-60.
20. F. Bergner and B. Köhler: *6th Eur. Conf. on Internal Friction and Ultrasonic Attenuation is Solids (ECIFUAS-6)*, Cracow, Poland, 1993, pp. 379-84.
21. F.J. Margetan, T.A. Gray, and R.B. Thompson: *Review of Progress in Quantitative NDE*, Plenum Press, New York, NY, 1991, vol. 10B, pp. 1721-28.
22. F.J. Margetan and R.B. Thompson: *Review of Progress in Quantitative NDE*, Plenum Press, New York, NY, 1992, vol. 11B, pp. 1717-24.
23. F.J. Margetan, R.B. Thompson, and I. Yalda-Mooshabad: *Review of Progress in Quantitative NDE*, Plenum Press, New York, NY, 1993, vol. 12B, pp. 1735-42.
24. I. Yalda-Mooshabad, F.J. Margetan, and R.B. Thompson: *Review of Progress in Quantitative NDE*, Plenum Press, New York, NY, 1993, vol. 12B, pp. 1727-35.
25. F.J. Margetan, R.B. Thompson, and I. Yalda-Mooshabad: *J. Nondestr. Eval.*, 1994, 13 (3), p. 111.

26. R.B. Thompson, F.J. Margetan, K.Y. Han, A.J. Paxson, and C.E. Shamblen: *Review of Progress in Quantitative NDE*, Plenum Press, New York, NY, 1992, vol. 11B, pp. 1685-91.
27. K.Y. Han, R.B. Thompson, F.J. Margetan, and J.H. Rose: *Review of Progress in Quantitative NDE*, Plenum Press, New York, NY, 1993, vol. 12B, pp. 1743-50.
28. J.H. Rose: *Review of Progress in Quantitative NDE*, Plenum Press, New York, NY, 1993, vol. 12B, pp. 1719-26.
29. J.H. Rose: *Review of Progress in Quantitative NDE*, Plenum Press, New York, NY, 1992, vol. 11B, pp. 1677-84.
30. J.H. Rose: *Review of Progress in Quantitative NDE*, Plenum Press, New York, NY, 1991, vol. 10B, pp. 1715-20.
31. W. Voigt: *Lehrbuch der Kristallphysik*, Tauber, Leipzig, 1928, p. 622.
32. A. Sigelmann and J.M. Reid: *J. Acoust. Soc. Am.*, 1973, vol. 53, pp. 1351-55.
33. E.L. Madsen, M.F. Insana, and J.A. Zagzebski: *J. Acoust. Soc. Am.*, 1984, vol. 76, pp. 913-23.
34. J.E. Gubernatis, E. Domany, J.A. Krumhansl, and M. Huberman: *J. Appl. Phys.*, 1977, vol. 48, p. 2812.
35. F.E. Stanke: Ph.D. Thesis, Stanford University, Stanford, CA, 1983.
36. F.E. Stanke: *J. Acoust. Soc. Am.*, 1986, vol. 80 (5), pp. 1479-85.
37. Y.K. Han: Ph.D. Thesis, Iowa State University, Ames, IA, 1994.
38. S. Ahmed and R.B. Thompson: *Review of Progress in Quantitative NDE*, Plenum Press, New York, NY, 1994, vol. 14, pp. 1617-24.